From cluster structures to nuclear molecules: The role of nodal structure of the single-particle wave functions

A. V. Afanasjev and H. Abusara

Phys. Rev. C **97**, 024329 — Published 23 February 2018

DOI: 10.1103/PhysRevC.97.024329

From cluster structures to nuclear molecules: the role of nodal structure of the single-particle wave functions.

A. V. Afanasjev[1] and H. Abusara[2]

[1]*Department of Physics and Astronomy, Mississippi State University, MS 39762*
[2]*Department of Physics, Birzeit University, Birzeit, Palestine*

(Dated: January 29, 2018)

The nodal structure of the density distributions of the single-particle states occupied in rod-shaped, hyper- and megadeformed structures of non-rotating and rotating $N \sim Z$ nuclei has been investigated in detail. The single-particle states with the Nilsson quantum numbers of the $[NN0]1/2$ (with N from 0 to 5) and $[N, N-1, 1]\Omega$ (with N from 1 to 3 and $\Omega = 1/2,\ 3/2$) types are considered. These states are building blocks of extremely deformed shapes in the nuclei with mass numbers $A \leq 50$. Because of (near)axial symmetry and large elongation of such structures, the wave functions of the single-particle states occupied are dominated by a single basis state in cylindrical basis. This basis state defines the nodal structure of the single-particle density distribution. The nodal structure of the single-particle density distributions allows to understand in a relatively simple way the necessary conditions for α-clusterization and the suppression of the α-clusterization with the increase of mass number. It also explains in a natural way the coexistence of ellipsoidal mean-field type structures and nuclear molecules at similar excitation energies and the features of particle-hole excitations connecting these two types of the structures. Our analysis of the nodal structure of the single-particle density distributions does not support the existence of quantum liquid phase for the deformations and nuclei under study.

PACS numbers: 21.10.Gv, 21.10.Pc, 21.60.Jz, 27.20.+n, 27.30.+t, 27.40.+z

I. INTRODUCTION

Recent years are characterized by the revival of the interest (both experimental and theoretical) to the study of cluster and extremely deformed structures in light nuclei (see Refs. [1–9] and references quoted therein). Many of these structures are described in terms of clusters, the simplest one being the α-particle [10, 11]. Cluster or similar type models provide an important insight into cluster dynamics of nucleus. However, the initial assumptions about clusters represent a limitation of this type of models and many shell model configurations are beyond of their reach. It is also important to remember that the cluster description does not correspond to clearly separated α-particles, but generates the mean-field states largely by antisymmetrization [11].

Alternative way of the description of exotic cluster configurations is within the framework of density functional theory (DFT) [4, 12, 13]. This type of models does not assume the existence of cluster structures but allows simultaneous treatment of cluster and mean-field-type states [4, 12–16]. In this framework, the formation of clusters proceeds from microscopic single-nucleon degrees of freedom via many-body correlations. Let us mention some recent studies of cluster and extremely deformed structures in the DFT framework. A linear chain of three α clusters, leading to "rod-shaped" nucleus and suggested about 60 years ago [17], was recently studied in the cranked relativistic mean field (CRMF) theory in Ref. [18]; its density distribution is presented in Fig. 1a. This exotic structure ("Hoyle" state) plays a crucial role in the synthesis of ^{12}C from three ^{4}He nuclei in stars [19]. Another example of rod-shaped nucleus is linear chain configuration of four α-clusters in ^{16}O. Recently the relationship between the stability of such states and angular momentum was investigated using Skyrme cranked Hartree-Fock (HF) method in Ref. [20] and CRMF approach in Ref. [16]. The cranked Skyrme HF framework was employed for the study of the stability of rod-shaped structures in highly-excited states of ^{24}Mg in Ref. [6].

However, the phenomenon of clusterization is not limited to the α-particles. Larger nuclei could play a role of building blocks of the clustered configurations. In particular, the nuclear configurations consisting of the $N = Z$ clusters with no or extra few valence nucleons could play an important role in the nuclei near the $N = Z$ line [10]. For example, the wave function of the superdeformed (SD) [2,2][1] band in ^{32}S contains a significant admixture of the molecular ^{16}O + ^{16}O structure [11, 21]. Extremely deformed structures such as super-, hyper- (HD) and megadeformed (MD) configurations as well as nuclear molecules have been systematically studied in the rotating $A = 28 - 50$ $N \approx Z$ nuclei in the CRMF framework (Refs. [9, 22]). A number of the configurations with cluster structures have been found in these calculations. Fig. 1(b-f) show some examples of such structures with different pattern of density distribution. The best example of nuclear molecule is the MD [421,421] configuration in ^{42}Sc (Fig. 1f) followed by the MD [42,42] configuration in ^{40}Ca (Fig. 1e) and the MD [31,31] configuration in ^{36}Ar (Fig. 1d). These three configurations show pronounced neck. On the other hand, the HD [2,2] configuration in ^{28}Si shows the clusterization at spin zero but

[1] The notation of the configurations is discussed in Sec. II.

with less pronounced neck (Fig. 1b). The rotation somewhat hinders these features and suppresses the neck in this configuration (see Fig. 1c and Ref. [22]).

In the DFT framework, the formation of clusters proceeds from microscopic single-nucleon degrees of freedom via many-body correlations. Although this fact is wildly recognized, in reality very little attention has been paid to the detailed study of the role of the single-particle states in clusterization. In that context, mostly the impact of the underlying single-particle and shell structure on the clusterization has been investigated. For example, the impact of underlying single-particle structure on the transition from spheroidal superdeformed configurations to doubly spherical configurations, which are analogs of cluster configurations, and the connection between the magic numbers at both shapes has been investigated in Ref. [23]. Even less attention has been paid to the structure of the single-particle wave functions and related single-particle densities and their impact on clusterization in the DFT framework. To our knowledge this has been discussed only in two publications. The formation of the total density of ^{8}Be nucleus from single-particle densities of occupied states has been discussed in Ref. [12]. The contribution of the single-particle densities of the [220]1/2 states into buildup of the ground state densities of ^{20}Ne has been presented in Ref. [4].

To address this gap in our knowledge of clusterization we perform systematic investigation of the densities of the single-particle states and their nodal structure in clustered and extremely deformed configurations of the $N = Z$ ^{12}C, ^{28}Si and ^{40}Ca nuclei. The selection of these nuclei is dictated by several factors. First, typical single-particle orbitals, which play a role at hyper- and megadeformation in the $N \approx Z$ nuclei with $Z = 6 - 24$, have to be considered. Second, the impact of reasonable changes of the nucleonic potential in axial and radial directions on the nodal structure of single-particle density distributions have to be investigated. Since nucleonic potential depends on total nucleonic density, this is achieved by considering nuclei which differ substantially in that respect. Note that the single-particle densities bear a clear fingerprint of underlying single-particle wave functions. Third, such choice of nuclei allows to see how significant is the impact of the lowering of the position of the single-particle orbital in nucleonic potential on the single-particle density distributions. In this paper we consider rotating and non-rotating nuclei and define which single-particle states favor the $\alpha-$clusterization, which states suppress this type of clusterization and which particle-hole excitations are important for the creation of nuclear molecules.

The difficulty in investigating cluster and extremely deformed states at spin zero is that they are generally unbound and lie at high excitation energies at low spins [10, 24]. Moreover, they are either formed on the shoulder or in very shallow minima of potential energy surfaces [12, 25]; thus, they are inherently unstable. The high density of nucleonic configurations at these energies and possible mixing among them is another factor hindering their experimental observation. As shown in Ref. [9], the rotation could help to overcome these obstacles. This is because extremely deformed configurations are favored by rotation at high spins (Refs. [9, 25, 26]) so that only such states could be populated above some specific spin values in the mass region of interest [9].

In the present paper the analysis is performed within the framework of covariant density functional theory (CDFT) [27]. It provides a fully self-consistent description of many nuclear phenomena. The CDFT well describes the experimental proton density distributions in spherical nuclei [28, 29], the deformations of superdeformed nuclei [30–33] and charge radii [34–36] across the nuclear chart. In addition, it provides good description of the changes in deformation and charge radii with the change of the configuration/particle number. These two facts strongly suggest that the CDFT properly reproduces the single-particle density contributions on which these observables depend[2]. This is an important factor in the context of the present investigation since the total density distribution (which could point either to α-clusterization or nuclear molecule) is built as a sum of the single-particle density distributions of occupied single-particle states. Note also that covariant (relativistic) energy density functionals (CEDFs) show more pronounced clusterization of the density distribution as compared with non-relativistic ones because of deeper single-nucleon potentials [4].

The studies of the single-particle densities in the present paper are also related to the general problem of the nucleon localization in finite nuclei. This problem was considered in Refs. [15, 37, 38], however, only total nucleon densities were used in the discussion of the localization. It was described in terms of different parameters reflecting different aspects of nuclear many-body problem. The α parameter representing the ratio of the spatial dispersion of the wave function to the average internucleon distance has been introduced in Ref. [37]. This parameter generally increases with the number of nucleons. Based on that, it was concluded that cluster states are more easily formed in light nuclei and that the transition from localized clusters to quantum liquid state occurs for nuclei with $A \approx 30$. An alternative localization measure has been employed in Refs. [15, 38]. It is defined as a conditional probability of finding a nucleon within a distance δ from a given nucleon at point $\mathbf{r}$ with the same spin and isospin. This measure has been applied both to light and very heavy nuclei.

The paper is organized as follows. Section II describes the details of the calculations. The basic features of the nodal structure of the single-particle wave function (and thus of its density distribution) in the case of extremely

[2] Note that at present there is no experimental technique which would allow to measure the density distribution of specific single-particle orbital (and thus its localization).

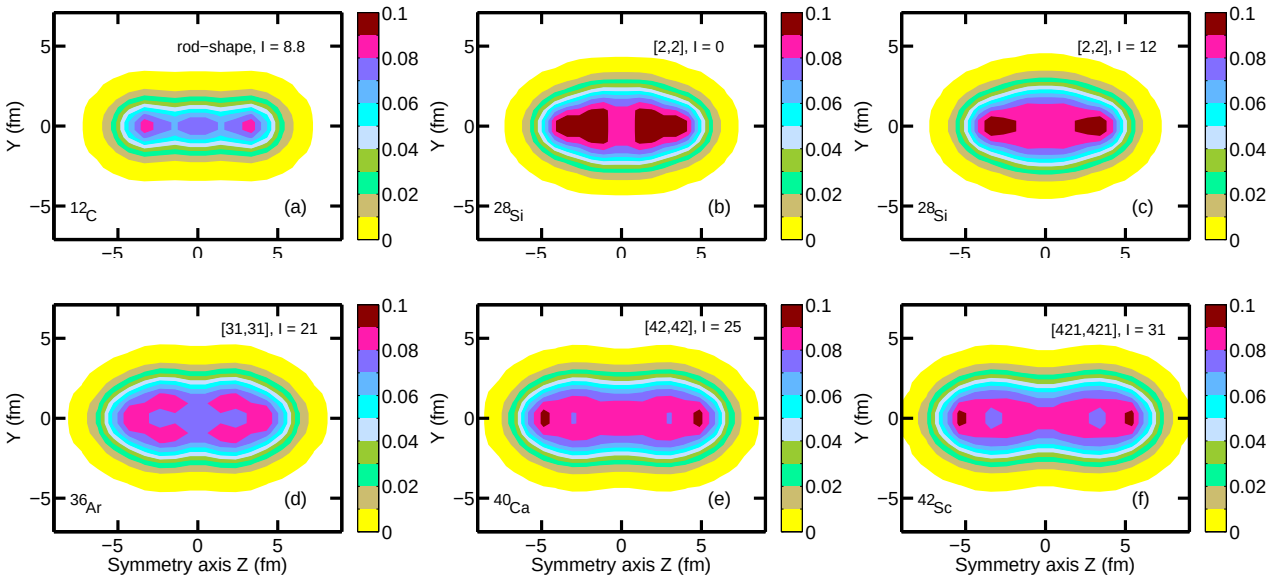

FIG. 1. (Color online) Total neutron densities [in fm^{-3}] of specified configurations in ^{12}C, ^{28}Si, ^{36}Ar, ^{40}Ca and ^{42}Sc at indicated spin values. The plotting of the densities starts with yellow color at 0.001 fm^{-3}. The densities presented in panels (b-f) are based on the results of the calculations of Ref. [9].

elongated prolate shapes are discussed in Sec. III. Secs. IV, V and VI analyse the densities and their nodal structures obtained in the CDFT calculations for the single-particle states occupied in rod-shaped structure of ^{12}C, hyperdeformed band of ^{28}Si and megadeformed structure of ^{40}Ca. Sec. VII summarizes the general features of the nodal structure of the single-particle density distributions and analyse how they affect the α-clusterization and the formation of nuclear molecules. Finally, Sec. VIII summarizes the results of our work.

II. THE DETAILS OF THE CALCULATIONS

The calculations are performed in the cranked relativistic mean field (CRMF) framework [27, 30] using the NL3* CEDF [39]. Note that one-dimensional rotation is along the x-axis in this framework. The pairing is neglected in the calculations since it has very little impact on the configurations of interest [9]. The CRMF equations are solved in the basis of an anisotropic three-dimensional harmonic oscillator in Cartesian coordinates, for details see Refs. [30, 40]. The truncation of basis is performed in such a way that all states belonging to the major shells up to $N_F = 14$ fermionic shells for the Dirac spinors and up to $N_B = 20$ bosonic shells for the meson fields are taken into account. This truncation scheme provides sufficient numerical accuracy (see Ref. [25] for details).

The calculated configurations are labeled by shorthand $[n_1(n_2)(n_3),p_1(p_2)(p_3)]$ labels, where n_1, n_2 and n_3 are the number of neutrons in the $N = 3$, 4 and 5 intruder/hyperintruder/megaintruder orbitals and p_1, p_2 and p_3 are the number of protons in the $N = 3$, 4 and 5 intruder/hyperintruder/megaintruder orbitals. If some of these orbitals are not occupied, the respective numbers are omitted in the configuration labels.

To give a full 3-dimensional representation of the single-particle density distributions, they are plotted in the figures below in the xz and yz planes at the positions of the Gauss-Hermite integration points in the y and x directions closest to zero. The density cross-section in the xy plane is taken at the Gauss-Hermite integration point in the z-coordinate which gives the largest density. The numerical values of these x and y coordinates are given in figure captions, while the value of the z coordinate is shown in middle panels of the figures which present single-particle density distributions. Note that some graphical results of the calculations are provided in the Supplemental Material with this article as Ref. [41].

III. THE NODAL STRUCTURE OF THE SINGLE-PARTICLE WAVE FUNCTION

Considering that the structures under investigation are characterized by the extreme prolate deformation and near axial symmetry (see Ref. [9]), the expansion of the wave functions of the single-particle states in terms of quantum numbers specific for asymptotic Nilsson quantum numbers (see Sec. 8.2 of Ref. [42]) is the most appropriate. Thus, the wave function $\Psi_{[Nn_z\Lambda]\Omega}$ of the single-

particle state denoted by the Nilsson quantum number[3] $[Nn_z\Lambda]\Omega$ is expanded into the basis states $|N'n'_z\Lambda'\Omega'>$ by

$$\Psi_{[Nn_z\Lambda]\Omega} = \sum_{N',n'_z,\Lambda',\Omega'} c_{N'n'_z\Lambda'\Omega'}|N'n'_z\Lambda'\Omega'> \quad (1)$$

Here, the basis states are characterized by principal quantum number N', the number n'_z of nodes in the axial direction (z-direction) and the projections of orbital (Λ') and total (Ω') single-particle angular momenta on the axis of symmetry. The sum in Eq. (1) runs over all allowable combinations of the quantum numbers N', n'_z, Λ' and Ω'.

Since the single-particle density $\rho_{[Nn_z\Lambda]\Omega}$ of the Nilsson state $[Nn_z\Lambda]\Omega$ is given by

$$\rho_{[Nn_z\Lambda]\Omega} = \sum_{N',n'_z,\Lambda',\Omega'} c^2_{N'n'_z\Lambda'\Omega'} < N'n'_z\Lambda'\Omega'|N'n'_z\Lambda'\Omega' > \quad (2)$$

the weights $c^2_{N'n'_z\Lambda'\Omega'}$ define the contributions of the basic states $|N'n'_z\Lambda'\Omega'>$ into the single-particle density.

The nodal structure of the single-particle wave function $\Psi_{[Nn_z\Lambda]\Omega}$ and thus of its density distribution is defined by the spatial part of the wave function. The spatial parts of the basis states are expressed in cylindrical (r, ϕ, z) coordinates in the following way (see Ref. [43] and Sec. 8.2 of Ref. [42])

$$|N'n'_z\Lambda' > \sim H_{n'_z}\left(\frac{z}{b_z}\right) L^{|\Lambda'|}_{n'_r}\left(\frac{r^2}{b^2_\perp}\right)\left(\frac{r}{b_\perp}\right)^{|\Lambda'|} e^{-\frac{1}{2}\left(\frac{z^2}{b^2_z}+\frac{r^2}{b^2_\perp}\right)} e^{i\Lambda'\phi} \quad (3)$$

where H and L are the Hermite and associated Laguerre polynomials. The b_z and $b_\perp$ are oscillator lenghts in axial and radial directions and n'_r is the number of radial nodes. The condition $N = n'_z + 2n'_r + |\Lambda'|$ defines the possible combinations of the quantum numbers n'_r, n'_z and Λ' and thus the nodal structure of the density distribution of the basis state.

The nodal structure in the axial direction of the wave function (Eq. (3)) and thus of related single-particle density distribution is defined by the zeros of the Hermite polynomials. In general, the nodal structure of density distribution in radial direction is defined by zeros in associated Laguerra polynomials and in the $\left(\frac{r}{b_\perp}\right)^{|\Lambda'|}$ term. It turns that all basis states (see Table I), providing the most important contributions to the wavefunctions of the single-particle states of interest, have $n_r = 0$ for which $L^{|\Lambda'|}_0\left(\frac{r^2}{b^2_\perp}\right) = 1$. With a single exception these states also have only two possible values of Λ', namely, 0 and 1. Thus, for these states the node at the axis of symmetry ($r = 0$) emerges only at $\Lambda' = 1$ from the $\left(\frac{r}{b_\perp}\right)^{|\Lambda'|}$ term. As a result, when considering the pattern of the density distribution only two types of the basis states are important, namely, the $|N, N, 0>$ and $|N, N-1, 1>$ states. The density distributions of the basis states with $|NN0>$ will be axially symmetric with the maximum of density located at the axis of symmetry. The basis states with $|N, N-1, 1>$ structure will have a zero density at the axis of symmetry.

However, as follows from Eq. (1) the basis states are expected to be mixed in the structure of the single-particle wave function. As a result, the single-particle wave functions may not have a well pronounced nodal structure specific for basis states. However, a number of factors leads to the reduction of such mixing in extremely deformed structures of light nuclei. First, the quality of asymptotic quantum numbers is improving with the increase of the elongation of the nuclear system (see Sec. 8.2 in Ref. [42]). In addition, such mixing depends on the energy distance between the basis states and the number of possible counterparts with which appreciable mixing could take place. At the bottom of nucleonic potential, these energy distances are large and the number of counterparts is quite limited (see Fig. 2). This leads to appreciable suppression of the mixing.

This is illustrated in Table I in which the weights $c^2_{N'n'_z\Lambda'\Omega'}$ of the three largest components of the wave functions of the single-particle states occupied in the megadeformed [42,42] configuration of ^{40}Ca are presented. One can see that the single-particle wave functions are dominated by a single very large component which in turn will define the spatial distribution of the single-particle density. This domination is especially pronounced at no rotation and for the single-particle orbitals located at the bottom of the nucleonic potential. Note that the [440]1/2 and [211]1/2 orbitals with $r = -i$ strongly interact in substantial frequency range near $\Omega_x \sim 1.8$ MeV (see Fig. 2b). This leads to an increase of the fragmentation of the wave function of these two states at $\Omega_x = 1.8$ MeV (Table I). However, such interaction is absent in the [440]1/2 and [211]1/2 orbitals with $r = +i$. As a result, their wave functions are substantially less fragmented (Table I).

It is interesting to compare the level of the fragmentation of the single-particle wave functions presented in Table I with the ones obtained in the calculations for other nuclei. Unfortunately, as a rule the studies within the cranking models based on different frameworks do not show detailed information on the structure of the single-particle wave functions. To our knowledge, there are only two exceptions which provide some hints on the fragmentation of the single-particle wave functions and their evolution with rotational frequency. The superdeformed bands in ^{32}S and neighboring odd-mass nuclei

[3] We use here the standard notation in which the single-particle states are labeled by the asymptotic quantum numbers $[Nn_z\Lambda]\Omega$ (Nilsson quantum numbers) of the dominant component of the wave function.

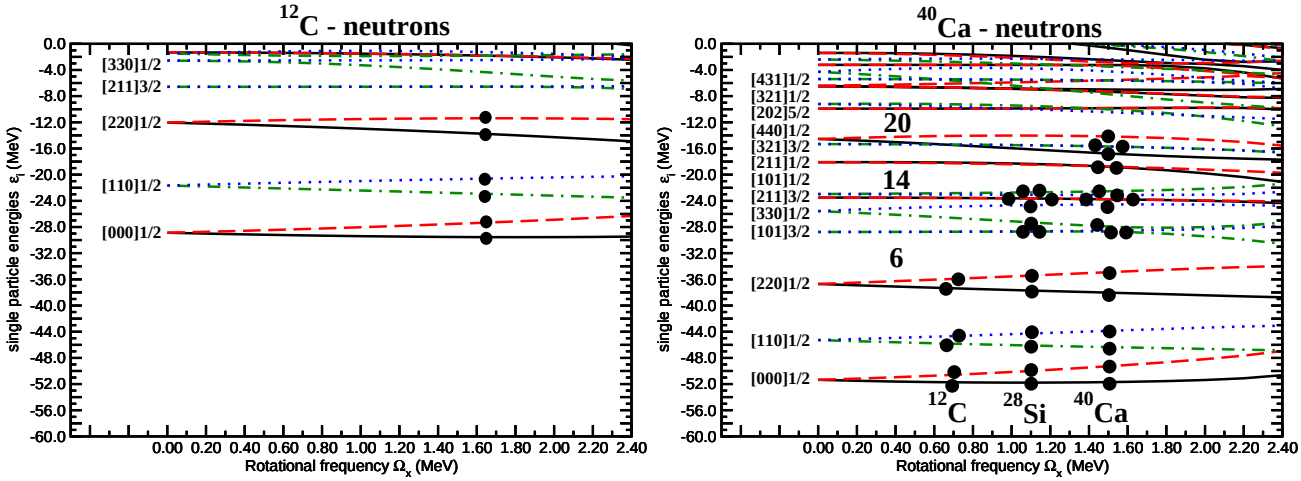

FIG. 2. (Color online) Neutron single-particle energies (routhians) in the self-consistent rotating potential as a function of the rotational frequency Ω_x. They are given along the deformation path of the rod-shaped structure in ^{12}C and yrast MD configuration [42,42] in ^{40}Ca. Long-dashed, solid, dot-dashed and dotted lines indicate ($\pi = +, r = +i$), ($\pi = +, r = -i$), ($\pi = -, r = +i$) and ($\pi = -, r = -i$) orbitals, respectively. At $\Omega_x = 0.0$ MeV, the single-particle orbitals are labeled by the asymptotic quantum numbers $[Nn_z\Lambda]\Omega$ (Nilsson quantum numbers) of the dominant component of the wave function. Solid circles indicate the occupied orbitals. Large shell gaps are indicated in the right panel.

have been studied in cranking Skyrme Hartree-Fock approach in Ref. [44]. The analysis of routhian diagrams presented in this manuscript indicate the change of the dominant components of the single-particle wavefunctions with rotational frequency for appreciable number of routhians which do not undergo unpaired band crossing. On the contrary, the rotation does not change the dominant components of the single-particle wave functions of the above mentioned type of the routhians shown in Table I. The substantial fragmentation of the single-particle wave functions has also been seen in the CRMF calculations of the yrast hyperdeformed configuration in ^{124}Xe [25]. Thus, the level of the fragmentation of the single-particle wave functions shown in Table I is on average substantially lower than the one seen in these two examples.

IV. ROD-SHAPE STRUCTURE IN ^{12}C

One of the examples of the cluster structures is the linear chain of three α-particles in ^{12}C [10]. These rod-shape structures in rotating ^{12}C and neighboring nuclei have been investigates in the framework of cranked relativistic mean field theory in Ref. [18]. The total neutron density distribution for this configuration in ^{12}C is presented in Fig. 1a and its routhian diagram is shown in Fig. 2a. The proton and neutron single-particle states with structure [000]1/2, [110]1/2 and [220]1/2 of both signatures are occupied in this configuration. Note that proton routhians are very similar to neutron ones; however, they are less bound (by roughly 8 MeV) because of the Coulomb interaction.

Single-particle density distributions of these states are shown in Fig. 3. One can see that they are almost axially symmetric (see density cross-sections in the xy-plane which is perpendicular to the symmetry axis z). The density distributions for opposite signatures of the specific orbital are almost the same. The same is also true for single-particle density distributions for the proton and neutron states with the same structure. Thus, it is sufficient to consider only neutron states with signature $r = +i$ as it is done in Fig. 3.

The density distributions of these states are almost axially symmetric with the maximum of density inside of each cluster located at the axis of symmetry. This is because their wave functions do not have nodes in radial direction. However, they show different nodal structure along the axis of symmetry since n_z is changing from 0 in the [000]1/2 state via 1 in the [110]1/2 state to 2 in the [220]1/2 state.

The density distribution of the [000]1/2 state, which is emerging from spherical $1s_{1/2}$ subshell, is the ellipsoid of revolution with the maximum of the density located at the center of nucleus. The density distribution of the [110]1/2 state, emerging from the spherical $1p_{1/2}$ subshell, is formed by two spheroids located symmetrically with respect of $z = 0$. The [220]1/2 orbital, emerging from spherical $1d_{5/2}$ subshell, shows three spheroidal clusters in density distribution; one of them is located at the center of nucleus and two others symmetrically with respect of it. Among these states, the highest localization of the wave function is seen in the [000]1/2 state. With increasing principal quantum number N (and the number of density clusters) the localization of the wave function and the maximum density in the center of the density cluster decreases.

The asymptotic Nilsson labels are quite good ap-

TABLE I. The squared amplitudes $c^2_{N'n'_z\Lambda'\Omega'}$ of three largest components of the wave functions of the single-particle states occupied in the megadeformed [42,42] configuration of ^{40}Ca. The states are shown from the bottom of nucleonic potential in the same sequence as they appear in the routhian diagram of this configuration (see Fig. 1b). The results are shown at no rotation (Ω_x = 0.0 MeV) and at rotational frequency Ω_x = 1.8 MeV which corresponds to spin $I = 25\hbar$. If not indicated otherwise, the orbitals have signature $r = -i$. Note that the [550]1/2 state is not occupied in this configuration.

State	Ω_x [MeV]	Wave function
[000]1/2	0.0	$92.7\%\|000,1/2> + 6.7\%\|220,1/2> + 0.4\%\|200,1/2>$
	1.8	$90.4\%\|000,1/2> + 8.7\%\|220,1/2> + 0.3\%\|200,1/2>$
[110]1/2	0.0	$89.6\%\|110,1/2> + 9.6\%\|330,1/2> + 0.4\%\|101,1/2>$
	1.8	$87.3\%\|110,1/2> + 9.6\%\|330,1/2> + 1.3\%\|101,3/2>$
[220]1/2	0.0	$85.1\%\|220,1/2> + 6.5\%\|000,1/2> + 6.2\%\|440,1/2>$
	1.8	$73.2\%\|220,1/2> + 8.9\%\|000,1/2> + 6.9\%\|440,1/2>$
[101]3/2	0.0	$92.9\%\|101,3/2> + 6.7\%\|321,3/2> + 0.3\%\|301,3/2>$
	1.8	$82.9\%\|101,3/2> + 9.4\%\|321,3/2> + 3.4\%\|101,1/2>$
[330]1/2	0.0	$75.7\%\|330,1/2> + 8.5\%\|110,1/2> + 6.8\%\|321,1/2>$
	1.8	$65.5\%\|330,1/2> + 8.9\%\|101,1/2> + 5.8\%\|101,3/2>$
[211]3/2	0.0	$92.5\%\|211,3/2> + 6.9\%\|431,3/2> + 3.6\%\|202,3/2>$
	1.8	$78.4\%\|211,3/2> + 7.2\%\|431,3/2> + 6.1\%\|220,1/2>$
[101]1/2	0.0	$90.2\%\|101,1/2> + 5.0\%\|330,1/2> + 4.4\%\|321,1/2>$
	1.8	$76.7\%\|101,1/2> + 7.2\%\|321,1/2> + 6.5\%\|330,1/2>$
[211]1/2	0.0	$81.4\%\|211,1/2> + 9.6\%\|431,1/2> + 5.2\%\|440,1/2>$
	1.8	$65.3\%\|211,1/2> + 22.1\%\|440,1/2> + 5.4\%431,3/2>$
[211]1/2	0.0	$81.4\%\|211,1/2> + 9.6\%\|431,1/2> + 5.2\%\|440,1/2>$
$(r = +i)$	1.8	$82.9\%\|211,1/2> + 6.8\%\|431,1/2> + 3.2\%\|211,3/2>$
[321]3/2	0.0	$85.7\%\|321,3/2> + 6.1\%\|101,3/2> + 6.0\%\|541,1/2>$
	1.8	$57.6\%\|321,3/2> + 9.1\%\|330,1/2> + 7.1\%\|312,5/2>$
[440]1/2	0.0	$77.4\%\|440,1/2> + 10.7\%\|211,1/2> + 4.1\%\|660,1/2>$
	1.8	$36.0\%\|440,1/2> + 20.3\%\|431,1/2> + 15.3\%\|211,1/2>$
[440]1/2	0.0	$77.4\%\|440,1/2> + 10.7\%\|211,1/2> + 4.1\%\|660,1/2>$
$(r = +i)$	1.8	$63.3\%\|440,1/2> + 15.2\%\|431,3/2> + 6.0\%\|220,1/2>$
[550]1/2	0.0	$79.3\%\|550,1/2> + 6.8\%\|541,1/2> + 6.7\%\|770,1/2>$
	1.8	$46.9\%\|550,1/2> + 23.9\%\|541,3/2> + 5.9\%\|770,1/2>$

proximate quantum numbers at the extreme deformations of interest (see also the discussion in Sec. 8.2 of Ref. [42]). For example, the lowest state in the routhian diagram has the structure $96.0\%|000,1/2> + 3\%|200,1/2> + 0.5\%|220,12> + ...$ at rotational frequency Ω_x = 0.0 MeV. Here and below we show only three largest squared components (in the format $c^2_{N'n'_z\Lambda'\Omega'}\%|N'n'_z\Lambda,'\Omega'>$) of the single-particle wave function. The rotation only somewhat modifies the structure of its wave function which at Ω_x = 3.2 MeV has the structure $92.5\%|000,1/2> + 3.0\%|200,1/2> + 2.8\%|220,1/2> + ...$ for the $r = -i$ branch. The same is true for other states of interest. The lowest negative parity state has the structure $94.6\%|110,1/2> + 4.0\%|310,1/2> + 0.4\%|101,1/2> + ...$ and $87.1\%|110,1/2> + 3.4\%[310,12> + 3.1\%|101,3/2> + ...$ (for the $r = -i$ branch) at Ω_x = 0.0 and Ω_x = 3.2 MeV, respectively. The lowest $N = 2$ state has the structure $89.7\%|220,1/2> + 5.8\%|420,1/2> + 1.5\%|211,1/2> + ...$ and $72.3\%|220,1/2> + 8.9\%|211,1/2> + 6.6\%|211,3/2> +...$ (for the $r = -i$ branch) at Ω_x = 0.0 and Ω_x = 3.2 MeV, respectively. Two general trends in the structure of the wave function are clearly seen on these examples. These are the increase of the fragmentation of the wave function (with related decrease of the dominant component of the wave function) with the raise of the position of the single-particle state with respect of the lowest state in the nucleonic potential and with increasing rotation of the nucleus. The first effect brings the state of interest into the region of increased density of the single-particle states and thus to the region where the interactions of the states are more abundant. The second is a consequence of the Coriolis interaction.

V. THE HYPERDEFORMED [2,2] CONFIGURATION IN ^{28}SI

Next we consider the hyperdeformed [2,2] configuration in ^{28}Si. The structure of this nucleus has been studied in detail in Ref. [22] where it was shown that this configuration is calculated at relatively low excitation energy at spins above $10\hbar$. Its total neutron density distribution is shown at spins $I = 0\hbar$ and $I = 12\hbar$ in Fig. 1(b-c). The HD [2,2] configuration shows clear signatures of clusterization which are especially pronounced at $I = 0\hbar$ (Fig. 1b). Although the rotation somewhat hinders these sig-

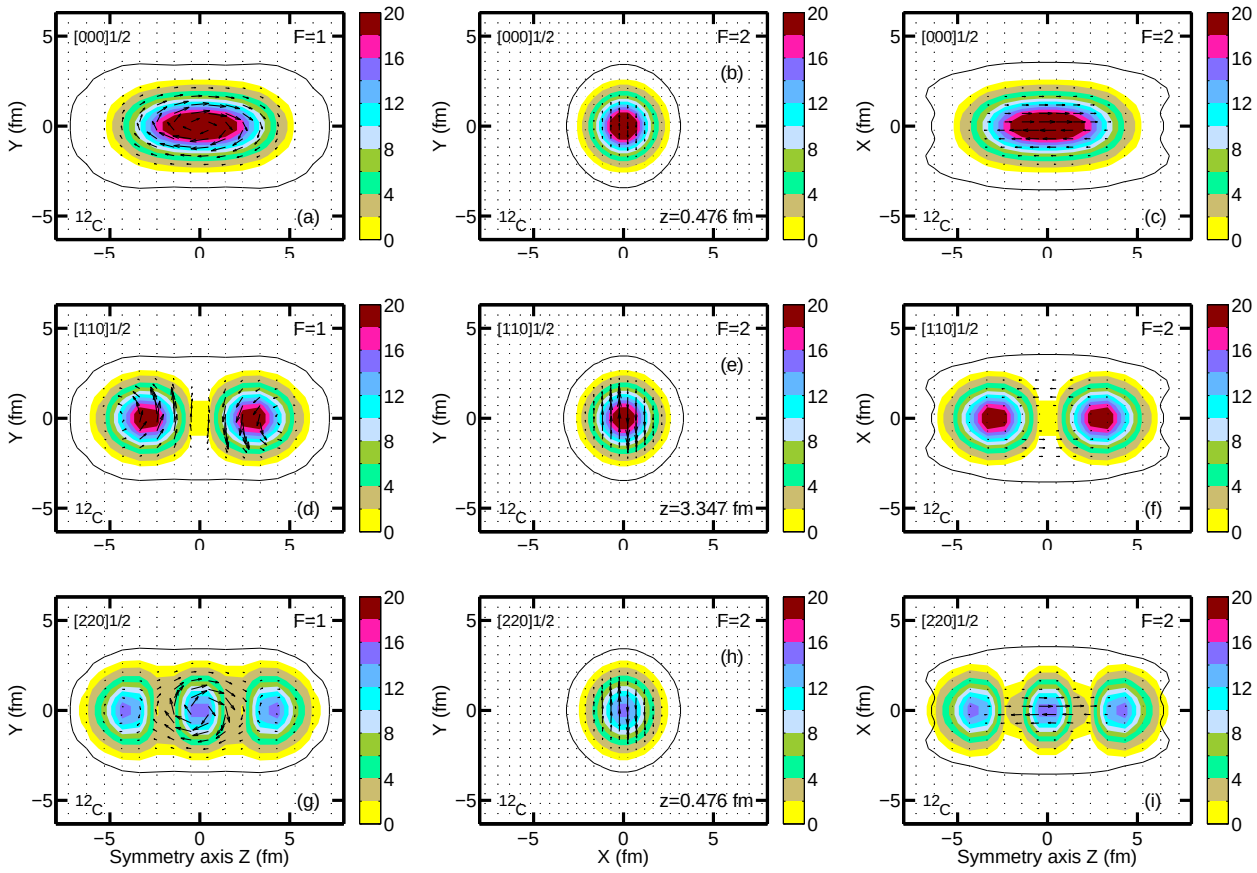

FIG. 3. (Color online) The single-neutron density distributions due to the occupation of the indicated Nilsson states with signature $r = -i$ in the rod-shape configuration of ^{12}C. The colormap shows the densities as multiplies of 0.001 fm^{-3}. The plotting of the densities starts with yellow color at 0.001 fm^{-3}. The results of the calculations are shown at rotational frequency $\Omega_x = 3.2$ MeV which corresponds to spin $I = 8.77\hbar$. For each state, the cross-sections in the yz and xz planes are plotted at $x = 0.234$ fm and $y = 0.234$ fm, respectively. The shape and size of the nucleus are indicated by black solid line which corresponds to total neutron density line of $\rho = 0.001$ fm^{-3}. In addition, the current distributions $\boldsymbol{j}^n(\boldsymbol{r})$ produced by these states are shown by arrows. The currents in panels (a),(d) and (g) are plotted at arbitrary units for better visualization. The currents in other panels are normalized to the currents in above mentioned panels by using factor F.

natures (Fig. 1c), they are still present at $I = 12\hbar$.

The length of the rod-shape structure in ^{12}C and the HD [2,2] configuration in ^{28}Si is almost the same in axial (z-) direction. However, the density of the HD [2,2] configuration is broader in the radial direction as compared with the one seen in rod-shape structure of ^{12}C. As follows from the discussion below, these differences are traced back mainly to the density distributions of the orbitals by which these two configurations differ.

The [000]1/2, [110]1/2 and [220]1/2 states are occupied both in the HD configuration of ^{28}Si and rod-shape structure of ^{12}C. Their density distributions and nodal structure are very similar in both nuclei (compare Fig. 3 with Figs. 1, 2 and 3 in the Supplemental Material [41]). However, the density distributions of these states in the HD [2,2] configuration of ^{28}Si are slightly less elongated in axial direction and somewhat more stretched out in radial direction as compared with the ones in rod-shape structure of ^{12}C. This is a consequence of two facts. First, the difference in total density distributions (rod-shape in ^{12}C versus ellipsoid like in ^{28}Si, Figs. 1(a-c)) affects the nucleonic potential. The sizes of the nuclei and thus of nucleonic potentials have also an impact. The charge radii of ^{12}C and ^{28}Si in the ground state are ~ 2.8 fm and ~ 3.15 fm, respectively (see Fig. 23 in Ref. [35]). However, these differences are compensated to a degree by the fact that these states are located deeper in the nucleonic potential of ^{28}Si (at single-particle energies $\varepsilon_i = -50.22, -40.20$ and -26.56 MeV at $\Omega_x = 0.0$ MeV for the [000]1/2, [110]1/2 and [220]1/2 states, respectively) as compared with the ones in ^{12}C (Fig. 2a) which leads to their smaller effective radius as compared with the radius of the ground state.

In addition, the Nilsson [101]3/2, [330]1/2, [211]3/2 and [101]1/2 orbitals are occupied in this configuration (see Fig. 2b). Their density distributions are presented in Figs. 4, 5 and 6 as well as in Fig. 4 of the Supplemental Material (Ref. [41]) at no rotation ($\Omega_x = 0.0$ MeV) and at

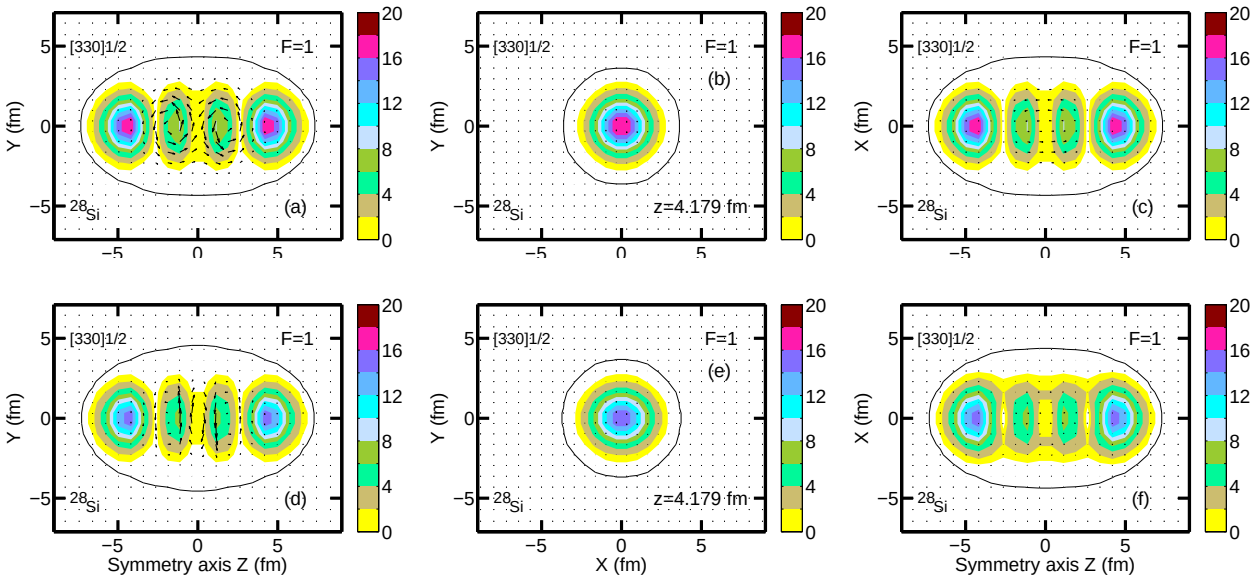

FIG. 4. (Color online) The same as Fig. 3 but for the $[330]1/2(r = -i)$ orbital in the HD [2,2] configuration of ^{28}Si. The densities in the yz and xz planes are taken at $x = 0.326$ fm and $y = 0.326$ fm, respectively. Top and bottom panels show the results at $\Omega_x = 0.0$ MeV and $\Omega_x = 1.8$ MeV, respectively.

rotational frequency $\Omega_x = 1.8$ corresponding to spin $I \sim 12\hbar$. The density distributions of these single-particle orbitals are characterized by different nodal structure.

The density distribution of the $[330]1/2$ orbital is similar in structure to the one seen for the $[NN0]1/2$ orbitals in ^{12}C and ^{28}Si: there are four density clusters located along the axis of symmetry with the maximum of the density in each cluster located at the axis of symmetry. The largest clusters with the highest density in the center are located in the polar region.

The orbitals with the Nilsson labels $[101]3/2$, $[101]1/2$ and $[211]3/2$ belong to the group of the states the wavefunctions of which are dominated by the basis states of the $|N, N-1, 1>$ type (see Table I). These basis states produce zero density at the axis of symmetry (see Sec. III). Significant reduction of the density on approaching the axis of symmetry is seen in the density distributions of these Nilsson states (see Figs. 5 and 6 in the manuscript and Fig. 4 in the Supplemental Material [41]). However, not always we see zero density at or close to the axis of symmetry. This is due to two reasons. First, there are the contributions into the wave functions emerging from the basis states of the $|NN0>$ type (see Table I) which build the density at the axis of symmetry. Second, because of calculational features the plots are made at the cross-sections which are located slightly off the axis of symmetry.

The $[101]1/2$ (Figs. 5(a-c)) and $[101]3/2$ (Figs. 4(a-c) in the Supplemental Material [41]) Nilsson states show very similar density distributions of doughnut type in which the maximum of the density is located in the equatorial plane. These two states at spin zero differ only in the orientation of the single-particle spin along the symmetry axis which has only moderate impact on the density distribution. As a result, their densities are similar at spin zero (compare Figs. 5(a-c) with Figs. 4(a-c) in the Supplemental Material [41]); minor differences are due to different single-particle energies and different projections Ω of the total single-particle angular momentum on the axis of symmetry which leads to the interaction of the single-particle states within the groups with different Ω (see Table I).

The wave function of the $[211]3/2$ Nilsson state is dominated by the $|211, 3/2>$ basis state the density of which has one node in radial direction and two nodes in axial direction. As a result, the density distribution of this Nilsson state is the combination of two circular axially symmetric density rings located symmetrically with respect of equatorial plane (Figs. 6(a-c)).

As illustrated in Table I the rotation leads to the modification of the structure of the wave function typically reducing the weight of its dominant component. Its impact depends on the state. For some states these modifications are rather small, for others they may be substantial. In general, the impact of the rotation on the single-particle densities can be characterized (i) by the change of their nodal structure, (ii) by the degree of delocalization of the wave function and (iii) by the change of their azimuthal dependence. For the states in the HD [2,2] configuration of ^{28}Si, the nodal structure of the single-particle density distributions is not affected by rotation. The rotation leads to some delocalization of the wave function which reflects itself in some increase of the space of the nucleus occupied by the particle [with related decrease of average density] and by some decrease of the maximum density in the density cluster (compare Figs. 4(a-c) and Figs. 4(d-

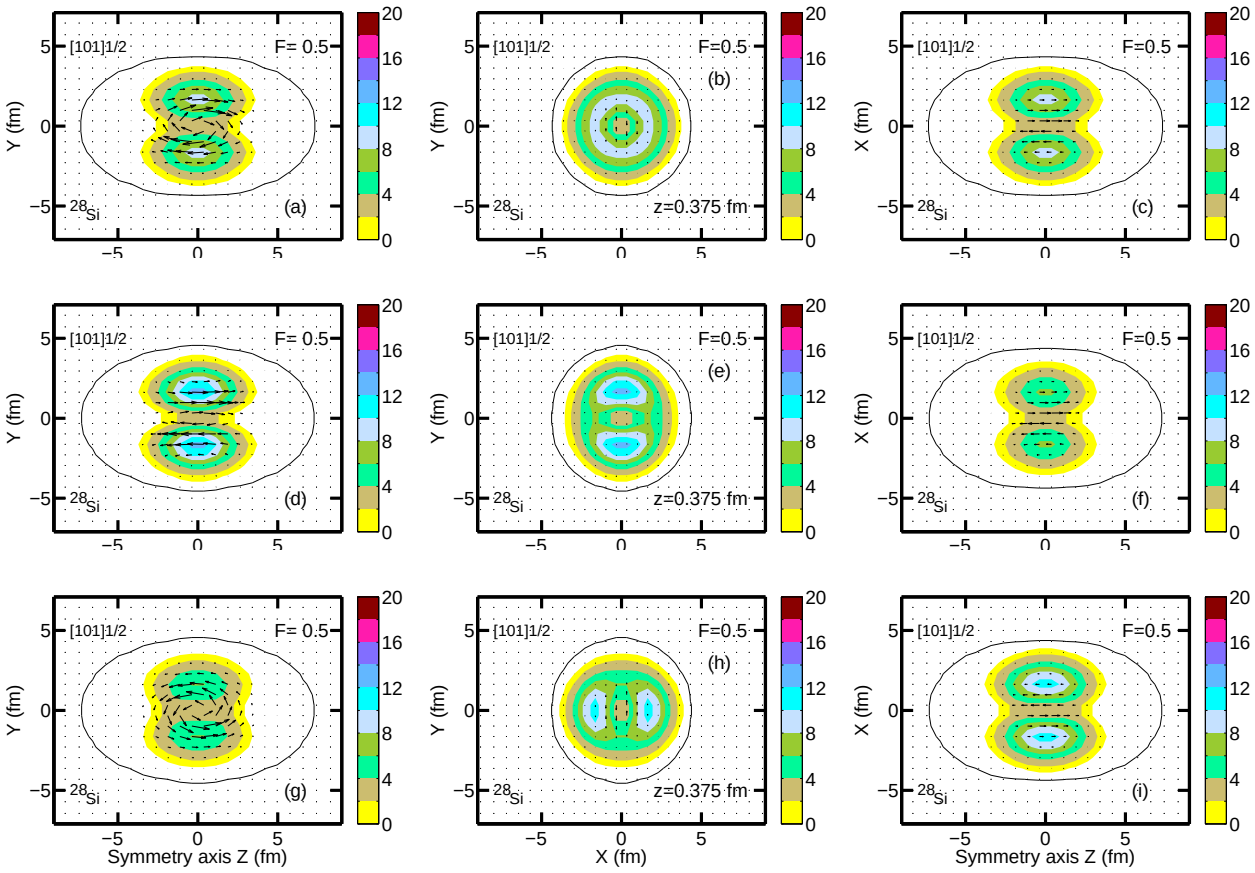

FIG. 5. (Color online) The same as Fig. 4 but for the $[101]1/2(r = \pm i)$ orbitals. The top panels show the results for the $(r = -i)$ orbital at $\Omega_x = 0.0$ MeV. Because the density distributions in both signatures of the [101]3/2 orbital are identical at $\Omega_x = 0.0$ MeV, the results for the $[101]3/2(r = +i)$ orbital are not shown here. Middle and bottom panels show the densities and currents at $\Omega_x = 1.8$ MeV for the $[\ 101]1/2(r = -i)$ and $[101]1/2(r = +i)$ orbitals, respectively.

f), compare upper, middle and bottom rows of Fig. 5 and of Fig. 4 in the Supplemental Material [41], compare upper and bottom rows in Fig. 6 and in Figs. 1, 2 and 3 of the Supplemental Material [41]). The changes in the azimuthal distribution of the densities induced by rotation are rather small for the $[NN0]1/2$ Nilsson states (see Fig. 4 and Figs. 1, 2 and 3 in the Supplemental Material [41]). On the other hand, they are quite substantial for the [101]1/2 (Fig. 5) and [101]3/2 (Fig. 4 in the Supplemental Material [41]) states. This is a consequence of the fact that the rotation leads to a different redistribution of the neutron matter for the $r = \pm i$ branches of the single-particle orbital resulting in an asymmetric doughnut density distributions in which the density depends on azimuthal angle. For example, the matter is moved away from the xz plane in the $\pm y$ directions for the $[101]1/2(r = -i)$ orbital [compare upper and middle panels of Fig. 5]. For the $[101]1/2(r = +i)$, this redistribution proceeds from the yz plane in the $\pm x$ direction [compare upper and bottom panels of Fig. 5]. Similar effect is also seen for the $[101]3/2(r = \pm i)$ states (Fig. 4 in the Supplemental Material [41]), but here it is inverted for $(r = \pm i)$ signatures as compared with the case of the $[101]1/2(r = \pm i)$ states. It is interesting that for the [101]1/2 and [101]3/2 states the rotation leads to the increase of maximum density in density cluster.

The observed features of the single-particle density distributions allow to understand in a simple way the transition from the rod-shape total neutron density in ^{12}C to the ellipsoid-like density distribution with two-pronounced clusters in ^{28}Si (Fig. 1). In ^{28}Si, six neutrons in the [000]1/2, [110]1/2 and [220]1/2 orbitals build the density distribution which is quite similar (slightly shorter in axial direction and slightly wider in radial direction) to the one seen in the rod-shape structure of ^{12}C (compare Fig. 7(b) with Fig. 7(a)). Thus, the 'rod-shape' cluster structure of ^{12}C (but with less pronounced central cluster) is still present in the HD [2,2] configuration of ^{28}Si. The addition of two neutrons into the [330]1/2 orbital will lead to some increase of the elongation of this substructure. However, the addition of six neutrons into the [101]1/2, [101]3/2 and [221]3/2 orbitals will lead to build up of the density at the radial coordinate away from the axis of symmetry located not far away from the equatorial plane. While the orbitals of the $[NN0]1/2$ type show the clusterization of the wavefunc-

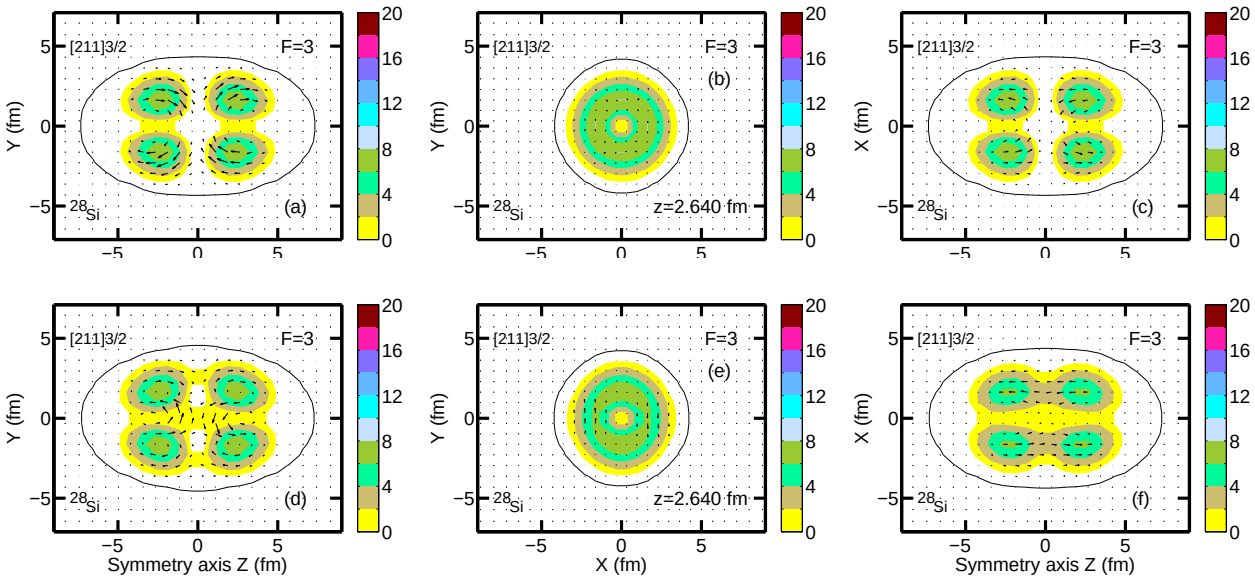

FIG. 6. (Color online) The same as Fig. 4 but for the $[211]3/2(r = -i)$ orbital.

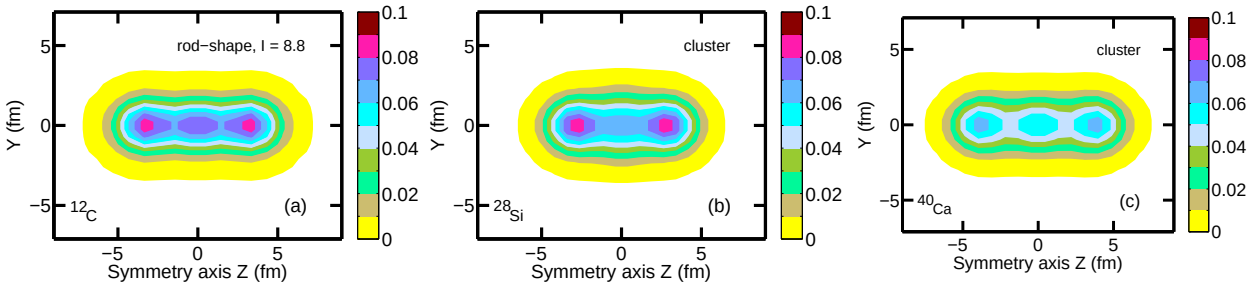

FIG. 7. (Color online) Total neutron densities produced by six neutrons occupying the lowest orbitals of the nucleonic potential, namely, [000]1/2, [110]1/2 and [220]1/2 in considered configurations of ^{12}C, ^{28}Si and ^{40}Ca. The plotting of the densities starts with yellow color at 0.001 fm^{-3}.

tion with substantial concentration of the density in at least one density cluster, the occupation of the [101]1/2, [101]3/2 and [221]3/2 orbitals with single radial node, leading to either doughnut or double axial ring structures, acts against α-clusterization. This is because they occupy substantial space of nucleus and are characterized by low density which even at its maximum is only slightly more than half of the maximum of the density seen in the density clusters produced by the orbitals of the $[NN0]1/2$ type. In addition, there is no a center of the density distribution in the [101]1/2, [101]3/2 and [221]3/2 orbitals which could be associated with α-particle.

VI. MEGADEFORMED [42,42] CONFIGURATION IN ^{40}CA.

Megadeformed [42,42] configuration in ^{40}Ca becomes yrast in the CRMF calculations at spin $I = 23\hbar$ [9]. It is more elongated with narrower neck than the HD [2,2] configuration in ^{28}Si (compare Fig. 1(e) with Figs. 1(b,c)). Despite these differences, the nodal structure of the densities of the single-particle states occupied below the $N = 14$ shell gap and their pattern of density distribution is the same for these two configurations in two nuclei (compare Figs. 4, 5, and 6 in the paper and Fig. 4 in the Supplemental Material (Ref. [41]) with Figs. 5 and 6 in the Supplemental Material [41]). Thus, we focus in this Section on the [211]1/2, [321]3/2 and [440]1/2 states which are located above the $N = 14$ shell gap and which are occupied in the MD [42,42] configuration of ^{40}Ca (Fig. 2).

In analogy to the case of the [101]1/2 and [101]3/2 states (see discussion in Sec. V), the density distributions of the [211]3/2 and [211]1/2 states are very similar at no rotation (compare Fig. 6 with Fig. 7 in the Supplemental Material [41]). The rotation affects the wave functions of the $(r = \pm i)$ branches of the [211]1/2 state in different way (see Table I). The wave function of the $r = +i$ orbital is only weakly affected by rotation so apart of the

modification of azimuthal dependence the nodal structure of its density distribution is the same as the one at no rotation (compare upper and bottom rows of Fig. 7 in the Supplemental Material [41]). On the contrary, at $\Omega_x = 1.8$ MeV the $r = -i$ orbital is strongly mixed with substantial admixture of the $|440, 1/2 >$ basis state (Table I). This leads to the emergence of the additional density cluster at axis of symmetry near $z \sim \pm 6$ fm (see middle row of Fig. 7 in the Supplemental Material [41]).

The wave function of the [321]3/2 state is dominated by the $|321, 3/2 >$ basis state which has one node in radial direction and two nodes in axial direction. As a result, the density distribution of this state is given by three density rings (Fig. 8); one is located in the equatorial plane and other two symmetrically with respect of this plane. At no rotation, these rings are almost axially symmetric. The rotation induces the dependence of the density on the azimuthal angle (azimuthal asymmetry); this is clearly seen in Fig. 8. For the $r = -i$ branch of this state, the density is mostly localized around the xz-plane and its vicinity (Fig. 8). The situation becomes reversed for the $r = +i$ branch, for which most of the density becomes localized around the yz-plane and its vicinity.

Fig. 9 displays the single-particle densities of the $[440]1/2(r = \pm i)$ orbitals and illustrates the impact of state mixing on the single-particle densities. The wave function of the $(r = +i)$ branch is dominated by the basis $|440, 1/2 >$ state (Table I). As a consequence, its density distribution closely follows to that expected for the $[NN0]1/2$ states, namely, five density clusters (which is a consequence of four $(n_z = 4)$ nodes in axial direction for the $|440, 1/2 >$ basis state) with the maximum of the density in each of them at the axis of symmetry (the consequence of no node in radial direction). The density distribution of the $(r = -i)$ branch is different since it is built from three spheroidal clusters (one at center and two in the polar regions) separated by the ring structure. The later comes from substantial admixture of the $|221, 1/2 >$ basis state which has this kind of density distribution (see, for example, Fig. 6 and bottom row in Fig. 5 of the Supplemental Material (Ref. [41]) as well as the discussion of the [221]3/2 state in ^{28}Si (Sec. V)).

VII. MAIN CONSEQUENCES OF THE NODAL STRUCTURE OF THE SINGLE-PARTICLE WAVE FUNCTIONS.

The analysis of the results of the CRMF calculations performed for extremely elongated shapes including hyperdeformed ones in ^{28}Si, megadeformed shapes in ^{40}Ca and rod-shape structures in ^{12}C reveals the following general features

- The buildup of such shapes from individual contributions of particles is defined by two groups of the single-particle states in the light nuclei with mass number A up to around 50. The states with the $[NN0]1/2$ structure belong to the first group[4] The second group is represented by the states with the $[N, N-1, 1]1/2$ and $[N, N-1, 1]3/2$ structures; note that the spatial distribution of the wave function (density) almost does not depend on Ω and is almost entirely defined by $[N, N-1, 1]$.

- With relatively few exceptions, the wave functions of the single-particle states occupied in such extremely deformed shapes are dominated by a single basis state. This is because the mixing of the basis states is suppressed at the bottom of nucleonic potential since the energy distances between the basis states which could mix are large and the number of possible counterparts with which appreciable mixing could take place is limited. Indeed, the fragmentation of the wave function (with related decrease of the dominant component of the wave function) typically increases with the raise of the position of the single-particle state with respect of the lowest state in the nucleonic potential.

- As a consequence, the nodal structure of the wave function (and thus of density distribution) of the single-particle state is defined solely by the nodal structure of the dominant basis state. However, the nodal structure of the density distribution of these basis states is determined by their quantum numbers. As a result, three basic types of single-particle density distributions, namely, spheroidal/elipsoidal shapes, doughnut and ring shapes, play an important role in forming the nuclear shapes at large elongation.

  - The density distributions of the Nilsson states with $[NN0]1/2$ quantum numbers are nearly axially symmetric with $N + 1$ spheroidal/elipsoidal like density clusters the maximum of the density of which is located at the axis of symmetry. With the exception of the $N = 0$ case, the clusters with highest densities are located in polar regions of the nuclei. This structure of the density distribution is the consequence of the nodal structure of the dominant basis state: no nodes in radial direction and $n_z = N$ nodes in axial direction.
  - The doughnut shapes are formed by the $[N01]\Omega$ states since the densities of their dominant basis states have one node in radial direction and no nodes in axial direction.

[4] Low energy structures in relatively light nuclei can be described in terms of molecular bonding [10]. For covalent bonding, a negative parity orbital perpendicular to the α-α axis is called a π-orbital, whereas a σ-orbital denotes a positive parity orbital parallel to the α-α direction. Thus, the [101]3/2 and [220]1/2 Nilsson states are the examples of the π- and σ-orbitals, respectively.

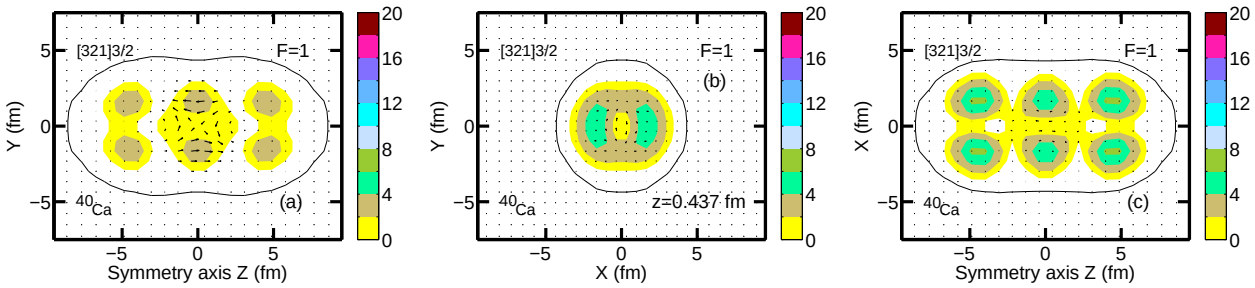

FIG. 8. (Color online) The same as Fig. 3 but for the $[312]3/2(r = -i)$ orbital in the MD [42,42] configuration of ^{40}Ca at rotational frequency $\Omega_x = 1.8$ MeV corresponding to spin $I = 25\hbar$. The densities in the yz and xz planes are taken at $x = 0.329$ fm and $z = 0.329$ fm, respectively.

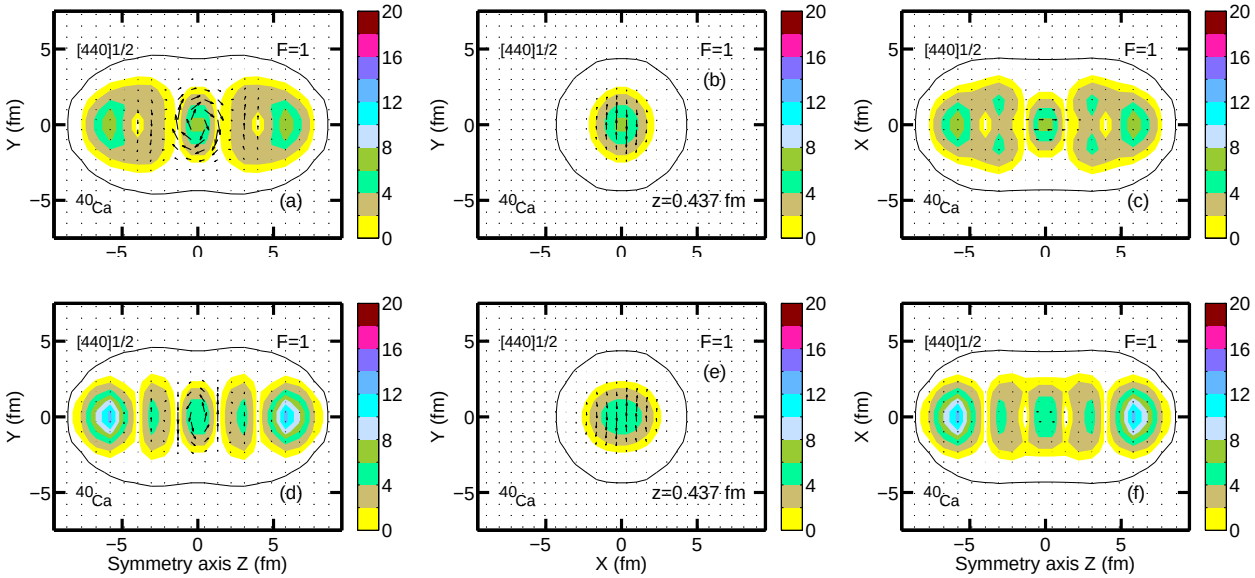

FIG. 9. (Color online) The same as Fig. 8 but for the $[440]1/2(r = \pm i)$ orbitals at $\Omega_x = 1.8$ MeV. Top and bottom panels show the results for the $(r = -i)$ and $(r = +i)$ branches, respectively. Note that the density distribution at $\Omega_x = 0.0$ MeV is very similar to what is seen in bottom panels.

  - Finally, the states with the structure $[N, N-1, 1]\Omega$ form multiply (two for $n_z = 1$ and three for $n_z = 2$) ring shapes for $N = 2$ and 3.

- Another source of increased fragmentation of the single-particle wave function is Coriolis interaction. It leads to some reduction of the weight of the dominant basis state in the single-particle wave function and to some delocalization of single-particle density. However, even with these effects accounted the single-particle states of interest for the rotational frequencies under study are dominated by a single basis state and their density distributions have the same nodal structure as the one at no rotation. Note that the rotation introduces some azimuthal dependence of the density distribution; this effect is especially pronounced for the states of the $[N, N-1, 1]$ type.

- The localization of the single-particle wave function strongly depends on its nodal structure. Only the states with low number of nodes in axial direction and with no nodes in radial direction could be well localized. The highest localization of the wave function is reached for the lowest states of the $[NN0]1/2$ type with $N = 0, 1$ and 2; that is a reason why these states are so important in α-clusterization. Subsequent increase of N and/or the number of the nodes in radial direction substantially decreases the level of the localization of the wave function. The rotation also reduces somewhat the localization of the wave function.

The structure of the clusters forming the nucleus is frequently defined in the DFT framework by comparing the density distributions of possible clusters with total density of the nucleus. Although some useful information can be obtained in that way, especially, with the use of the localization functions defined in Refs. [15, 38]

such an approach has its own limitations. This measure of localization is inherently defined for total quantities because the nucleon localization function considers the conditional probability of finding a nucleon within a distance δ from a given nucleon at point $\mathbf{r}$ with the same spin σ and isospin τ [15, 38, 45]. Thus, it cannot be applied to the single-particle quantities. As a result, the present analysis suggests an alternative way in which the single-particle densities forming the total density of the nucleus and its constituent clusters are compared. Since single-particle densities bear a clear mark of the underlying single-particle wave functions, such way of the comparison can provide a microscopic understanding on how the nucleus is formed from the clusters. The work on that type of the analysis is in the progress and the results will be presented in a forthcoming publication.

A. Nodal structure of the single-particle densities and the transition to liquid phase

The analysis of Ref. [37] based on the consideration of total nucleonic densities and harmonic oscillator potential has suggested that the nuclei heavier than $A \sim 30$ consist of largely delocalized nucleons. As a result, the transition from coexisting cluster and mean-field states to a Fermi liquid state should occur for nuclei with $A \approx 20 - 30$ [37]. Note that for solid phase, the nuclear configurations are characterized by the situation in which each particle is localized with respect of its neighbours [46]. On the contrary, the individual particles are delocalized in a quantum liquid [46, 47]. By definition the quantum liquid is many-body system whose behaviuor is defined by the effects of both quantum mechanics and quantum statistics [48]. The latter enters into the game through the requirement of the indistinguishability of the constituent particles ([48]) which defines the type of quantum statistics (Fermi or Bose). This requirement cannot be satisfied in finite nuclei if the occupied states are localized and have different spatial distributions.

The analysis of the single-particle densities performed in the present paper suggests that the transition to quantum liquid does not happen in the considered nuclei. Although with the increase of particle number the occupation of the single-particle orbitals with lower level of localization becomes dominant, none of these states can be described as delocalized. They still preserve their nodal structure and typically occupy less than half of the volume of the nucleus.

B. α-clusterization and its evolution with particle number

The observed features of the single-particle density distributions emerging from the nodal structure of the wavefunctions allow to understand in a relatively simple way the necessary conditions for α-clusterization. Two factors play an important role here: the degree of the localization of the wavefunction and the type of the density clusters formed by single-particle orbital. It is clear that for the α-clusterization the single-particle density clusters should be compact (well localized), should have spheroidal or slightly elipsoidal density distribution and overlap in space. These conditions are satisfied only for the lowest states of the $[NN0]1/2$ type with $N = 0, 1$ and 2 which are active in the α-cluster structures of very light nuclei [4, 10, 18, 23, 49]. With increasing particle number the orbitals with doughnut and multiply ring type density distributions become occupied. These states are substantially less localized; the maximum of the density in such structures is typically much smaller than the maximum of the density in the lowest $[NN0]1/2$ orbitals. In addition, such density distributions (doughnuts and rings) are incompatible with α-clusters.

Based on these considerations it is clear that α-clustering in highly elongated nuclear structures for typical deformations considered here should be an important mode only in very light nuclei in which the states of the $[NN0]1/2$ type are occupied. Although the α-cluster substructures still survive in heavier nuclei (Fig. 7), their contribution to the total wave function of the nucleus is expected to decrease as compared with light nuclei with increasing mass number because of increased contribution of the single-particle structures with ring- and doughnut-type density distributions. This trend is similar to the one obtained in antisymmetrized molecular dynamics calculations of Ref. [11].

C. Building nuclear molecules by means of particle-hole excitations

The coexistence of ellipsoidally shaped structures and nuclear molecules in the same nucleus has been seen in the CRMF calculations of Ref. [9] for similar elongations of nuclear shape. It turns out that the configurations of these two types of the shapes are connected by characteristic particle-hole excitations. A specific feature of the nuclear molecules is the existence of two fragments connected by the neck. The MD configurations [31,31] in ^{36}Ar, [42,42] in ^{40}Ca and $[421, 421]$ in ^{42}Sc (Fig. 1d-f) are the examples of nuclear molecules (Ref. [9]). To build nuclear molecules from typical elipsoidal density distributions one has to move the matter from the neck (equatorial) region into the polar regions of the nucleus. This can be achieved by specific particle-hole excitations[5] removing particles from (preferentially) doughnut type orbitals or from the orbitals which have a density ring in

[5] Note that particle-hole excitations are a powerful tool of the modification of the density distribution in finite nuclei. For example, they can substantially modify the radial dependence of matter distribution in spherical nuclei [50] or introduce a deformation into nuclear system [42].

a equatorial plane into the orbitals (preferentially of the $[NN0]1/2$ type) which build the density mostly in the polar regions of the nucleus.

The results presented in Ref. [9] give a number of examples of such particle-hole excitations leading to the transitions from elipsoidal nuclear shapes to nuclear molecules. One such an example is the transition from the HD [4,4] configuration in ^{36}Ar, which has ellipsoidal density distribution [see Fig. 24b in Ref. [9]]), to the MD [31,31] configuration which is an example of nuclear molecule [see Fig. 24c in Ref. [9] and Fig. 1d in the present paper]. This transition involves the proton and neutron particle-hole excitations from the 3/2[321] orbital (which has triple ring density distribution) into the $[440]1/2(r = -i)$ orbital. Another example is the transition from the [41,41] configuration in ^{42}Sc, which has ellipsoidal density distribution (see Fig. 8a in Ref. [9]), to the MD [421,421] configuration which is a very good example of nuclear molecule (Fig. 1f). This transition is achieved in proton and neutron subsystems by the particle-hole excitations from the [202]5/2 (which has doughnut type density distribution) and [321]3/2 (which has triple ring density distribution) orbitals into the $[440]1/2(r = +i)$ and $[550]1/2(r = +i)$ orbitals. The latter orbitals have the largest and most dense density clusters in the polar regions of the nucleus (see Fig. 9 and Fig. 8 in the Supplemental Material [41]).

D. The currents and rigid rotation of the system

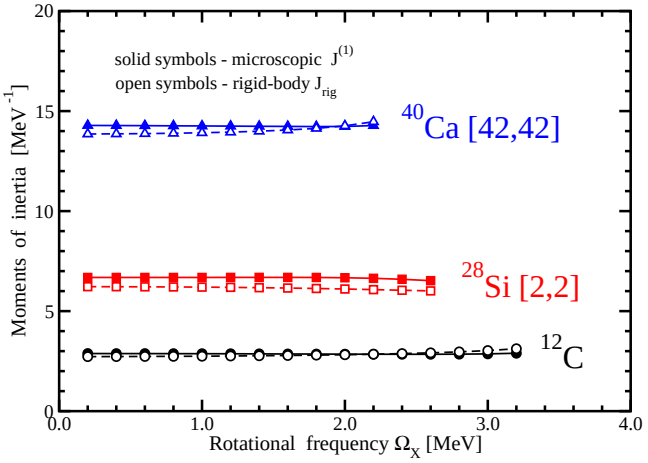

FIG. 10. (Color online) The calculated moments of inertia for the indicated configurations.

Fig. 10 compares microscopically calculated kinematic moments of inertia $J^{(1)}$ with the rigid body moments of inertia J_{rig} for the configurations under study. $J^{(1)}$ is calculated fully self-consistently via

$$J^{(1)}(\Omega_x) = \frac{J}{\Omega_x}, \tag{4}$$

where J is the expectation value of the total angular momentum along the x-axis and Ω_x is rotational frequency along the same axis. In the CRMF framework, J is defined as a sum of the expectation values of the single-particle angular momentum operators $\hat{j}_x$ of the occupied states

$$J = \sum_i \langle i|\hat{j}_x|i\rangle. \tag{5}$$

Note that the effects of the time-odd mean fields, which are extremely important for the moments of inertia (see Refs. [51, 52]), are included fully self-consistently in the CRMF calculations.

The rigid body moment of inertia J_{rig} is obtained in one-dimensional cranking approximation with the rotation defined around the x-axis from the calculated density distribution $\rho(\mathbf{r})$ by

$$J_{rig} = \int \rho(\mathbf{r})(y^2 + z^2)d^3r \tag{6}$$

An interesting feature of the rotating bands in the nuclei under consideration is the fact that their microscopic kinematic moment of inertia $J^{(1)}$ changes very little with the increase of rotational frequency. Indeed, the variation of $J^{(1)}$ over calculated rotational frequency is only 0.47%, 2.4% and 0.4% of its total value in rotational bands of ^{12}C, ^{28}Si and ^{40}Ca, respectively[6]. The rigid body moment of inertia is rather close to the microscopic one; it deviates from $J^{(1)}$ by -5.3% ($+7.8\%$), -6.9% (-7.8%) and -3.0% ($+1.3\%$) of the $J^{(1)}$ value at the lowest (highest) calculated frequencies for the rotational bands of ^{12}C, ^{28}Si and ^{40}Ca, respectively. Note that similar analysis for the hyperdeformed bands in the $Z = 40-58$ region shows that microscopic and rigid body moments of inertia differ typically by less than 5% (Ref. [52]). This difference is bigger in ^{12}C and ^{28}Si most likely due to smaller number of the single-particle orbitals involved as a result of which their individual features still play a prominent role in the definition of the total properties of the configuration. In any case, these differences between microscopic and rigid body moments of inertia are significantly smaller than those expected in normal-deformed bands (see Ref. [52]). Thus, the bands under study behave in a first approximation like rigid rotors.

The microscopic origin of these features can be traced back to underlying shell structure. Indeed, the analysis within the periodic orbit theory [53] for superdeformed rotational bands shows that the single-particle orbitals that cause shell structure of prolate superdeformed nuclei do not carry rotational flux if the axis of rotation is perpendicular to the symmetry axis. Therefore, the moments of inertia of such rotational bands should be

[6] This is not general feature since the kinematic moments of inertia show pronounced variations in a number of configurations (see Fig. 35 in Ref. [9]).

equal to the rigid-body value [53]. Based on general arguments this conclusion has to be valid also for prolate hyperdeformed and megadeformed bands. Such conclusion is supported by our microscopic calculations which show that the calculated moments of inertia of extremely deformed rotational bands are typically within 5% of the rigid-body value in the medium mass nuclei (Ref. [52]) and close to this value in light nuclei (as defined in the present manuscript).

The distributions of the total neutron currents in the yz plane are shown in Fig. 11. They are defined as [52]

$$\boldsymbol{j}^n(\boldsymbol{r}) = \sum_{i=1}^{N} (\psi_i(\boldsymbol{r}))^\dagger \hat{\boldsymbol{\alpha}} \psi_i(\boldsymbol{r}). \quad (7)$$

where $\psi_i(\boldsymbol{r})$ are the single-neutron wave functions. Thus, total current is built as a sum of the individual currents $\psi_i(\boldsymbol{r}))^\dagger \hat{\boldsymbol{\alpha}} \psi_i(\boldsymbol{r})$ of the occupied orbitals. These individual currents are shown in the figures with single-particle density distributions (see Figs. 3, 4, 5, 6, 8, 9, and the figures in the Supplemental Material [41]). Note that the yz plane is perpendicular to the axis of the rotation. As a result, in general the currents in this plane are substantially larger than the ones in the xz and xy planes and they show the vortices. Note that the localization, the strength, and the structure of the current vortices created by a particle in a specific single-particle state depend on its nodal structure (for more details see Sec. V in Ref. [52], Ref. [54] and Sec. III C in Ref. [55]). All single-particle states are characterized by the weak current in the surface area and neither of them shows the current distribution expected for rigid rotation.

It is well known that there are no currents in the intrinsic frame if the rigid nonspherical body rotates uniformly (rigid rotation) (see Sec. IV A-V in Ref. [56]). The presence of strong current vortices in Fig. 11 demonstrates the dramatic deviation of the currents from rigid rotation. This is despite the fact that the moments of inertia of considered configurations are close to the rigid-body value. This fact underlines the importance of quantum mechanical treatment of the currents.

The experimental data on the moments of inertia can be easily extracted from the rotational sequences of observed states. However, the discussion in this section as well as the results obtained within periodic orbit and cranked relativistic mean field theories in Refs. [52, 53] show that the closeness of experimental moment of inertia to the rigid body value is not sufficient indicator of the rigid-body rotation. To confirm or reject such an interpretation one should measure the currents but they are not experimentally accessible quantities.

VIII. CONCLUSIONS

In conclusion, the nodal structure of the density distributions of the single-particle states occupied in extremely deformed structures (such as rod-shaped, hyper- and megadeformed ones) of non-rotating and rotating $N \sim Z$ nuclei has been investigated in detail. Such structures are either axial or nearly axial in the CRMF calculations and they are present in light nuclei with $Z = 4 - 24$ [9, 16, 18, 22]. This simplifies the situation and with relatively few exceptions the wave functions of the single-particle states occupied in such extremely deformed shapes are dominated by a single basis state. As a consequence, the nodal structure of the wave function (and thus of the density distribution) of the single-particle state is defined solely by the nodal structure of this dominant basis state, the structure of which is given by the Nilsson label $[Nn_z\Lambda]\Omega$. Two types of the states, namely, $[NN0]1/2$ (with N from 0 to 5) and $[N, N-1, 1]1/2$ $(N, N-1, 1]3/2)$ (with N from 1 to 3) define the features of extremely deformed configurations in the nuclei under study.

For extremely deformed shapes in the $A \leq 50$ nuclei considered here, the nodal structure of the single-particle states does not depend on the nucleonic configuration (occupation of the single-particle states) or rotation. The only exception is the case of strong interaction of two single-particle states with the same parity and signature which leads to the mixing of the wavefunctions of interacting orbitals and thus of their single-particle densities. However, this happens rarely and in limited rotational frequency range.

The observed features of the single-particle density distributions emerging from the nodal structure of the wavefunctions allow to understand in a relatively simple way the necessary conditions for α-clusterization and the suppression of the α-clusterization with the increase of mass number. In addition, it allows to understand the coexistence of ellipsoidal mean-field type structures and nuclear molecules at similar excitation energies and the features of particle-hole excitations connecting these two types of the structures.

Our investigation shows that although with increasing the particle number the occupation of the single-particle orbitals with low level of localization of the single-particle densities becomes dominant, the states sitting deep in the nucleonic potential still remain well localized. In addition, neither of the occupied states lose their nodal structure and become delocalized. Thus, for the deformations and nuclei under study no transition to quantum liquid phase has been observed.

IX. ACKNOWLEDGEMENTS

This material is based upon work supported by the U.S. Department of Energy, Office of Science, Office of Nuclear Physics under Award No. DE-SC0013037.

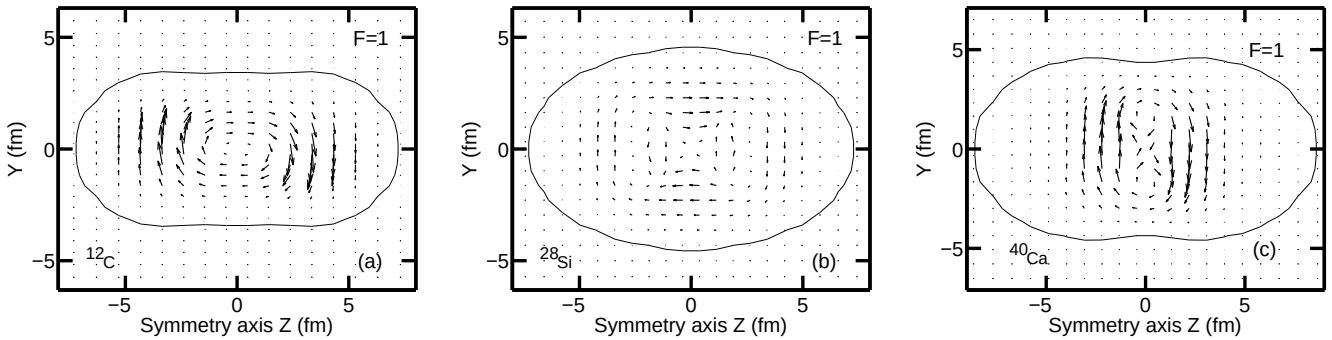

FIG. 11. (Color online) Total neutron currents $\boldsymbol{j}^n(\boldsymbol{r})$ in the yz plane plotted at $x = 0.234$ fm, $x = 0.326$ fm and $x = 0.329$ fm for the considered configurations in ^{12}C, ^{28}Si and ^{40}Ca, respectively. They are given at spin values indicated in Fig. 1. The currents in panel (a) are plotted at arbitrary units for better visualization. The currents in other panels are normalized to the currents in above mentioned panels by using factor F.

[1] Y. Taniguchi, Y. Kanada-En'yo, M. Kimura, K. Ikeda, H. Horiuchi, and E. Ideguchi, Phys. Rev. C **82**, 011302 (2010).
[2] Y. Kanada-En'yo, Phys. Rev. C **85**, 044320 (2012).
[3] Y. Taniguchi, Phys. Rev. C **90**, 054308 (2014).
[4] J.-P. Ebran, E. Khan, T. Nikšić, and D. Vretenar, Nature **487**, 341 (2012).
[5] E. Epelbaum, H. Krebs, T. A. Lähde, D. Lee, and U.-G. Meißner, Phys. Rev. Lett. **109**, 252501 (2012).
[6] Y. Iwata, T. Ichikawa, N. Itagaki, J. A. Maruhn, and T. Otsuka, Phys. Rev. C **92**, 011303 (2015).
[7] M. Kimura, T. Suhara, and Y. Kanada-En'yo, Eur. Phys. J. **A52**, 373 (2016).
[8] E. F. Zhou, J. Yao, Z. Li, J. Meng, and P. Ring, Phys. Lett. B **753**, 227 (2016).
[9] D. Ray and A. V. Afanasjev, Phys. Rev. C **94**, 014310 (2016).
[10] W. von Oertzen, M. Freer, and Y. Kanada-En'yo, Phys. Rep. **432**, 43 (2006).
[11] J. A. Maruhn, M. Kimura, S. Schramm, P.-G. Reinhard, H. Horiuchi, and A. Tohsaki, Phys. Rev. C **74**, 044311 (2006).
[12] J.-P. Ebran, E. Khan, T. Nikšić, and D. Vretenar, Phys. Rev. C **90**, 054329 (2014).
[13] J.-P. Ebran, E. Khan, T. Niksic, and D. Vretenar, Journal of Physics G: Nuclear and Particle Physics **44**, 103001 (2017).
[14] J. L. Egido and L. M. Robledo, Nucl. Phys. A **738**, 31 (2004).
[15] P.-G. Reinhard, J. A. Maruhn, A. S. Umar, and V. E. Oberacker, Phys. Rev. C **83**, 034312 (2011).
[16] J. M. Yao, N. Itagaki, and J. Meng, Phys. Rev. C **90**, 054307 (2014).
[17] H. Morinaga, Phys. Rev. **101**, 254 (1956).
[18] P. W. Zhao, N. Itagaki, and J. Meng, Phys. Rev. Lett. **115**, 022501 (2015).
[19] F. Hoyle, Astr. J. Suppl. **1**, 121 (1954).
[20] T. Ichikawa, J. A. Maruhn, N. Itagaki, and S. Ohkubo, Phys. Rev. Lett. **107**, 112501 (2011).
[21] M. Kimura and H. Horiuchi, Phys. Rev. C **69**, 051304 (2004).
[22] A. V. Afanasjev and D. Ray, J. Phys: Conf. Ser. **863**, 012502 (2017).
[23] S. Åberg and L.-O. Jönsson, Z. Phys. A **349**, 205 (1994).
[24] D. Jenkins, J. Phys. G **43**, 024003 (2016).
[25] A. V. Afanasjev and H. Abusara, Phys. Rev. C **78**, 014315 (2008).
[26] J. Dudek, K. Pomorski, N. Schunck, and N. Dubray, Eur. Phys. J **A20**, 15 (2004).
[27] D. Vretenar, A. V. Afanasjev, G. A. Lalazissis, and P. Ring, Phys. Rep. **409**, 101 (2005).
[28] Y. K. Gambhir, P. Ring, and A. Thimet, Ann. Phys. (N.Y.) **198**, 132 (1990).
[29] L. R. Gasques, A. V. Afanasjev, E. F. Aguilera, M. Beard, L. C. Chamon, P. Ring, M. Wiescher, and D. G. Yakovlev, Phys. Rev. C **72**, 025806 (2005).
[30] A. V. Afanasjev, J. König, and P. Ring, Nucl. Phys. A **608**, 107 (1996).
[31] A. V. Afanasjev, P. Ring, and J. König, Nucl. Phys. **A676**, 196 (2000).
[32] A. V. Afanasjev, I. Ragnarsson, and P. Ring, Phys. Rev. C **59**, 3166 (1999).
[33] E. Ideguchi, D. G. Sarantites, W. Reviol, A. V. Afanasjev, M. Devlin, C. Baktash, R. V. F. Janssens, D. Rudolph, A. Axelsson, M. P. Carpenter, A. Galindo-Uribarri, D. R. LaFosse, T. Lauritsen, F. Lerma, C. J. Lister, P. Reiter, D. Seweryniak, M. Weiszflog, and J. N. Wilson, Phys. Rev. Lett. **87**, 222501 (2001).
[34] L. Geng, H. Toki, and J. Meng, Prog. Theor. Phys. **113**, 785 (2005).
[35] S. E. Agbemava, A. V. Afanasjev, D. Ray, and P. Ring, Phys. Rev. C **89**, 054320 (2014).
[36] A. V. Afanasjev and S. E. Agbemava, Phys. Rev. C **93**, 054310 (2016).
[37] J. P. Ebran, E. Khan, T. Niksic, and D. Vretenar, Phys. Rev. C **87**, 044307 (2013).
[38] C. L. Zhang, B. Schuetrumpf, and W. Nazarewicz, Phys. Rev. C **94**, 064323 (2016).
[39] G. A. Lalazissis, S. Karatzikos, R. Fossion, D. P. Arteaga, A. V. Afanasjev, and P. Ring, Phys. Lett. **B671**, 36 (2009).
[40] W. Koepf and P. Ring, Nucl. Phys. A **493**, 61 (1989).

[41] See Supplemental Material at [URL will be inserted by publisher] for the results of the calculations not included into main body of the manuscript.
[42] S. G. Nilsson and I. Ragnarsson, *Shapes and shells in nuclear structure*, (Cambridge University Press, 1995).
[43] S. G. Nilsson, Mat.-Fys. Medd.-K.Dan. Vidensk. Selsk. **29**, 16 (1955).
[44] H. Molique, J. Dobaczewski, and J. Dudek, Phys. Rev. C **61**, 044304 (2000).
[45] A. D. Becke and K. E. Edgecombe, J. Chem. Phys. **92**, 5397 (1990).
[46] B. R. Mottelson, Nucl. Phys. A **649**, 45c (1999).
[47] D. Pines and P. Nozieres, *The theory of Quantum Liquids* (Benjamin, Elmsford, NY, 1966).
[48] A. J. Leggett, *Quantum Liquids. Bose Condensation and Cooper Pairing in Condensed-Matter Systems* (Oxford University Press, Oxford, 2006).
[49] M. Freer, R. R. Betts, and A. H. Wuosmaa, Nucl. Phys. A **587**, 36 (1995).
[50] A. V. Afanasjev and S. Frauendorf, Phys. Rev. C **71**, 064318 (2005).
[51] J. König and P. Ring, Phys. Rev. Lett. **71**, 3079 (1993).
[52] A. V. Afanasjev and H. Abusara, Phys. Rev. C **82**, 034329 (2010).
[53] M. A. Deleplanque, S. Frauendorf, V. V. Pashkevich, S. Y. Chu, and A. Unzhakova, Phys. Rev. C **69**, 044309 (2004).
[54] P. Gulshani and D. J. Rowe, Can. J. Phys. **56**, 480 (1978).
[55] A. V. Afanasjev and H. Abusara, Phys. Rev. C **81**, 014309 (2010).
[56] A. Bohr and B. R. Mottelson, *NUCLEAR STRUCTURE Volume II: Nuclear Deformation* (W. A. Benjamin, Inc., 1975).